Tumor location is a major determinant of macromolecular transport, collagen fiber morphology, and metastasis

Marie-France Penet[1], Samata Kakkad[1], Arvind P. Pathak[1], Venu Raman[1], Meiyappan Solaiyappan[1], and Zaver M. Bhujwalla[1]

[1]*JHU ICMIC Program, The Russell H. Morgan Department of Radiology and Radiological Science, The Johns Hopkins University School of Medicine, Baltimore, MD, United States*

Introduction: Lymphatic metastasis and malignant ascites are major causes of poor prognosis and quality of life in prostate cancer patients. Cancer cells metastasize more readily from orthotopic sites than from heterotopic sites (1). Here we have focused on characterizing the role of the extracellular matrix (ECM) in allowing lymphatic and ascites metastatic dissemination from metastasis-permissive environments and on understanding the role of hypoxia in these environments using noninvasive MR and optical imaging of orthotopic and subcutaneous tumor xenografts. MRI of the macromolecular contrast agent (MMCA) albumin-GdDTPA was used to characterize interstitial fluid transport, second harmonic generation (SHG) microscopy of tissue slices to determine collagen fiber distribution, and green fluorescent protein (GFP) expression to detect hypoxia. Intrinsic SHG signal in tumors is primarily from collagen I fiber, which is a major component of the ECM in tumors. These studies will provide insights into the dynamics governing interstitial transport, and the influence of collagen I fiber in these dynamics, within these metastasis-permissive environments.

Methods: PC3-HRE-EGFP cells were engineered to express enhanced green fluorescent protein (EGFP) under hypoxia as previously described (2). For orthotopic implantation, we used a microsurgical method that avoids disseminating cancer cells during inoculation in the prostate (3). Intact PC3-HRE-EGFP tumor tissue grown in the flank of severe combined immunodeficient (SCID) male mice ($<1mm^3$) was implanted in the prostate by suturing it into the lobes of the gland of anesthetized SCID male mice. By implanting tissues rather than injecting cells, the stromal tissue and the three dimensional cytoarchitecture, believed to play a critical role in tumor progression and metastasis, were maintained. Volume matched tumor tissue was also implanted subcutaneously in a separate group of mice. All MR imaging was performed on a Bruker Biospec 4.7T spectrometer when the tumors were approximately 300-400 mm^3. The mice were anesthetized with a mixture of ketamine and acepromazine. The tail vein was catheterized before placing the animal in the magnet. Interstitial fluid transport parameters were measured from quantitative T_1 maps obtained before and after intravenous administration of the contrast agent albumin-GdDTPA (500 mg/kg dose). Images were acquired in two "phases" corresponding to the biphasic kinetics of the macromolecular contrast agent (MMCA) (3). The "early phase" images obtained over the initial 30 min were used to characterize the tumor vasculature. Since drainage of macromolecules in and around tumors either by convection or by lymphatics is a slow event, the second block of MR data was acquired up to 123 min post contrast and was used to characterize interstitial transport of the MMCA. Interstitial fluid transport parameters derived included the number of draining and pooling voxels, draining and pooling rates and exudate volumes as previously described (4). Following MRI, SHG microscopy of fresh tissue slices slices was performed with multiphoton imaging on a Zeiss 710 LSM NLO microscope system at 880 nm excitation and 25x magnification. 3 D image stacks were acquired from randomly selected fields of view. Collagen fiber morphology was characterized in terms of the inter-fiber distance and fiber volume using an in-house 3D analysis tool that identified collagen fibers based on their tubular geometry (5).

Results and Discussion: Orthotopic tumors were identified from their higher signal intensity in diffusion-weighted images, as shown in **Figure 1A**. A significant increase of pooling voxels was observed in orthotopic compared to subcutaneous tumors (**Figures 1B and D**). No significant differences were observed in the number of draining voxels (**Figures 1C and D**). Efflux and influx rates were lower in orthotopic tumors (**Figure 1E**). The total pooling volume tended to be higher in the orthotopic tumors (**Figure 1F**). Representative SHG images of collagen I inter-fiber distance and fiber volume are shown in **Figure 2** and demonstrate a significantly higher fiber density and volume in orthotopic tumors. Metastases to lymph nodes, lungs (**Figure 3**) and several other organs were routinely observed following orthotopic implantation, but rarely occurred after subcutaneous implantation. Overall, orthotopic prostate tumors were characterized by a higher density of collagen fibers, a higher number of pooling voxels, and lower efflux and influx rates compared to subcutaneous tumors. Characterization of hypoxia in orthotopic and subcutaneous environments and its relationship to interstitial transport and collagen fiber distribution is ongoing. These data demonstrate the profound impact of the location of tumor growth on the ECM and macromolecular transport, and provide additional insights into environments that are permissive for metastasis and the accumulation of malignant ascites.

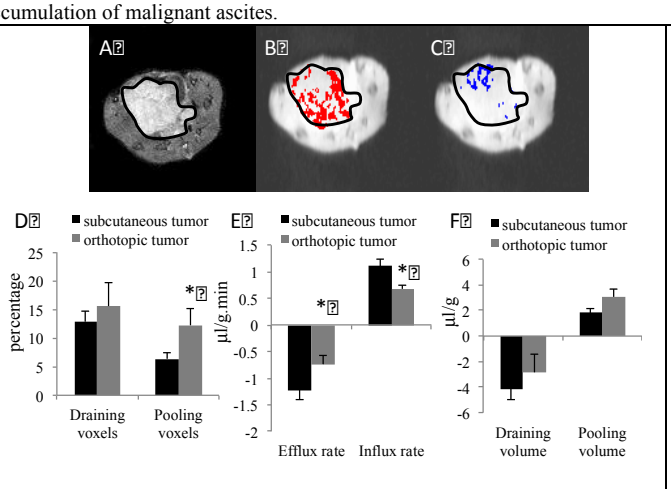

Figure 1: (A) Representative diffusion-weighted image, **(B)** map of pooling voxels and **(C)** map of draining voxels obtained from an orthotopic tumor. Bar graphs showing **(D)** the percentage of draining and pooling voxels, **(E)** the efflux and influx rates and **(F)** the pooling and draining volumes in subcutaneous (n=7) and orthotopic (n=6) tumors (*p<0.05).

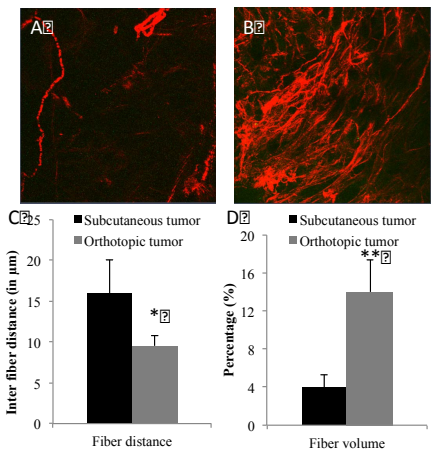

Figure 2: Representative collagen I fiber patterns from **(A)** subcutaneous and **(B)** orthotopic tumors. Bar graphs of **(C)** inter-fiber distance and **(D)** fiber volume in subcutaneous (n=5) and orthotopic (n=4) tumors (*p<0.05, **p<0.001).

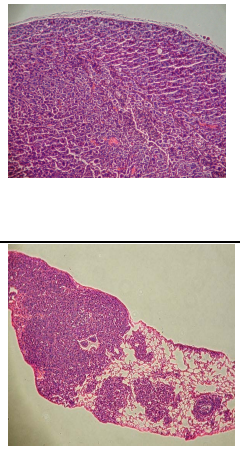

Figure 3: Lymph node entirely invaded by cancer cells (top row) and metastatic nodules in lung (bottom row) following orthotopic implantation.

Acknowledgement: This work was supported by NIH P50 CA103175 and R01 CA73850. **References:** (1) Penet *et al*, Cancer Res, 69:8822-9, 2009. (2) Raman *et al*, Cancer Res, 66:9929-9936, 2006. (3) An *et al.*, Prostate, 34:169-74, 1998. (4) Pathak *et al*, Cancer Res, 65:1425-32, 2005. (5) Kakkad *et al*, Neoplasia 12:608-17, 2010.